# On the origin of the difference between type A and type B skeletal isomerization of alkenes catalyzed by zeolites : the crucial input of ab initio molecular dynamics

Jerôme Rey, Axel Gomez, Pascal Raybaud, Céline Chizallet, Tomáš Bučko

# On the origin of the difference between type A and type B skeletal isomerization of alkenes catalyzed by zeolites: the crucial input of ab initio molecular dynamics

*Jérôme Rey,[1] Axel Gomez,[1] Pascal Raybaud,[1] Céline Chizallet,[1,*] Tomáš Bučko,[2,3]**

[1] IFP Energies nouvelles – Rond-Point de l'Echangeur de Solaize – BP 3 69360 Solaize, France

[2] Department of Physical and Theoretical Chemistry, Faculty of Natural Sciences, Comenius University in Bratislava, Ilkovičova 6, SK- 84215 Bratislava, Slovakia

[3]Institute of Inorganic Chemistry, Slovak Academy of Sciences, Dúbravská cesta 9, SK-84236 Bratislava, Slovakia

Corresponding authors: celine.chizallet@ifpen.fr ; bucko19@uniba.sk

**ABSTRACT**

Alkene skeletal izomerisation elementary steps catalyzed by acid zeolites are key reactions in refining, petrochemistry and biomass conversion. We unravel the atomic-scale origin of the higher rate constant of type A isomerization (involving a direct alkyl transfer, without any change in the branching degree) than the one of type B isomerization (involving non-classical carbonium ions such as protonated cyclopropane (PCP), inducing a change in the branching degree) of $C_7$ carbenium ions in chabazite. Accurate free energy barriers are calculated at 300 and 500 K for both reactions by means of molecular dynamics in combination with blue moon ensemble approach, whereas the static approach is shown to fail to describe these reactions. The slow transformation between individual rotational isomers, causing non-ergodic sampling of reactant state, largely overlooked in literature, is carefully addressed in the present work. At 500 K (representative of experimental conditions), free energy barriers of 83.4 kJ/mol and 15.0 kJ/mol are determined for type B and type A isomerization respectively. The much lower barrier for type A is thus recovered, and assigned to a loose transition state, with free rotation of the migrating alkyl group, while the transition state of type B isomerization is tighter, with such a rotation blocked, due to the simultaneous hydride shift taking place on the edge of the PCP.

**KEYWORDS**: carbenium; protonated cyclopropane; blue moon ensemble; chabazite; rotamers.

# 1. INTRODUCTION

Carbenium chemistry is at the core of a large set of chemical transformations in organic chemistry [1–6], with crucial current and prospective industrial repercussions. As a major example, the bi-functional isomerization of alkyl chains is a key reaction in refining [7,8], petrochemistry [8,9] and biomass conversion [10–12]. Hydrocracking and hydroisomerization are among the major industrial current processes based on carbenium chemistry. They are utilized for instance in production of diesel and jet fuels from conventional fossil resources [13], in technologies making use of the heaviest parts of hydrocarbons obtained via the Fischer-Tropsch process from different feedstock (coal, biomass or gas), or for very heavy unconventional crudes such as tar sands and shale oils [14,15]. Hydrocracking and hydroisomerization catalysts typically combine two functions: a hydrogenation/dehydrogenation function on a noble metal or a metallic sulfide and an acidic function of the Brønsted type provided by zeolites or amorphous silica-aluminas [15].

A sequence of reactions taking place in these processes begins by the dehydrogenation of alkanes into alkenes. The alkenes are protonated afterwards on the acidic function. Intermediate carbocations are formed and these species evolve by isomerization and β-scission reactions. The resulting shorter and isomerized alkenes are hydrogenated to form alkanes, which are eventually desorbed as products [15,16]. The isomerization reactions of alkenes are typically catalyzed by acid zeolites at temperatures around 250 °C and at a partial pressure of $H_2$ of around 1-10 bars [15,16].

The isomerization is classified as type A when it does not lead to any branching degree change (in practice, this corresponds to a direct hydride or 1,n alkyl transfer [17]), or type B when an increase in the branching degree of the chain occurs. These transformations involve non-classical carbonium ions such as protonated cyclopropane (PCP) [8,17–19]. The latter are often invoked for type B isomerization but are also likely to be relevant in the case

of type A alkyl-shifts. Type B isomerization reactions are of interest when cracking is aimed at, as higher branching degree is expected to allow the preferential formation of tertiary or secondary carbenium ions (instead of primary ones) favoring easier cracking [8,20]. It is known that type A isomerization is several orders of magnitude faster than type B isomerization [8,15–17,21]. However, the molecular origin of such a ranking is still poorly understood. Moreover, the intermediate *versus* transition state nature of the PCP is debated for a long time [22]. Earlier static ab initio calculations dealing with zeolites suggest that it should be a transition state [23–28], but the determination of the energy profile was biased by the alkoxide nature of the reactants and products, whereas more recent *ab initio* molecular dynamics showed that, at finite temperature, tertiary carbenium ions exist in significant concentrations [29,30]. Finally, determining accurately the intrinsic free energy barrier for type A and type B isomerization reactions is rather challenging, as the isomerization reactions generally occur simultaneously, and together with hydrogenation-dehydrogenation reactions, plus cracking. Single-event kinetic schemes were successful in fitting experimental data in that respect, and also in reproducing the expected trend according to which type A is faster than type B [31–35]. However, considering the number of adjustable parameters in these models, quantifying the intrinsic free energy barriers for these elementary steps by an independent approach is called for.

Herein, we report a density functional theory (DFT) investigation addressing these issues. We analyze the free energetics of type B isomerization connecting a $C_7$ dibranched tertiary cation (2,4-dimethyl-pent-2-enium cation) to a tribranched tertiary cation (2,3,3-trimethyl-but-2-enium cation) and we compare the free energy barriers with those of type A isomerization involving the same tribranched tertiary cation (Figure 1). The model reactions studied herein are the "building blocks" for the key elementary steps of the hydroisomerization of alkanes, in practice however, the rate constants of these individual

steps are not easy to quantify. Lumping of steps is usually performed in single-event kinetic modeling approach, which prevents a detailed mechanistic analysis. As a model for the catalyst, the acid chabazite zeolite is considered in this work. In the literature, the finite temperature effects are most often introduced via static approach to the transition state theory (TST) consisting of atomic relaxations followed by calculations of harmonic vibrational frequencies, which are subsequently employed in approximate formulae for free energy, enthalpy, and other thermodynamic quantities of interest. Previous theoretical work [36–38], however, demonstrated that such a simple approach can not provide satisfactory results for free energy analysis of hydrocarbon conversions in zeolites. Free energy methods based on molecular dynamics (MD) [29,30,36–46] or Monte Carlo (MC) simulations [47,48], which are designed to study chemical reactions, are free of limitations of the static approach. Due to their high computational cost and a non-trivial realization, the use of these methods in theoretical catalysis is still rather limited. To the best of our knowledge, they were never used for the type A versus type B isomerization of alkenes.

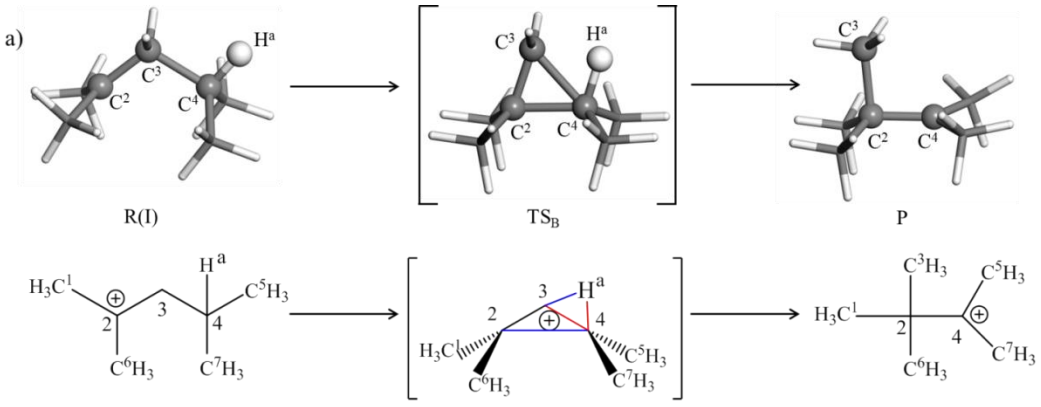

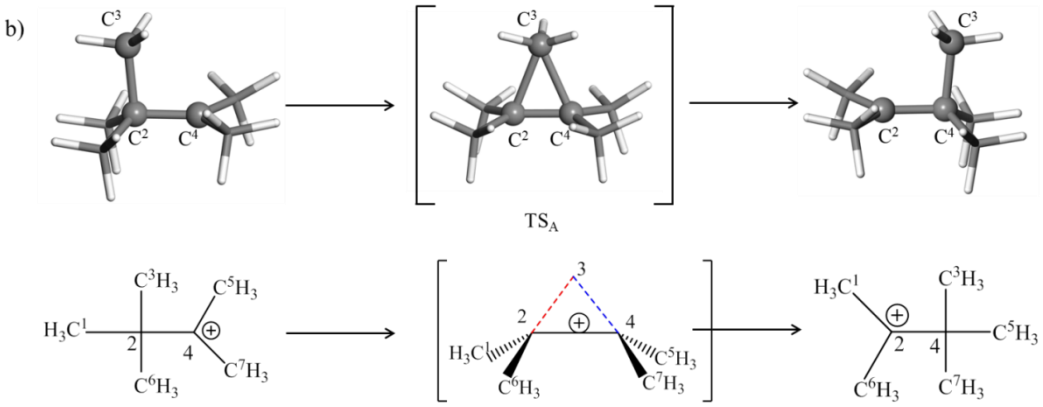


**Figure 1.** Isomerization reactions: a) type B between 2,4-dimethyl-pent-2-enium cation and 2,3,3-trimethyl-but-2-enium cation, b) type A between two symmetry equivalent 2,3,3-trimethyl-but-2-enium cations. Note that the reactant of reaction b) is identical with the product of reaction a). The ball and sticks structures are optimized in gas phase. The blue and red lines indicate the bonds that are, respectively, formed and broken during the reactions.

We investigate these mechanisms with advanced *ab initio* molecular dynamics methods (blue moon ensemble approach), that we compare with a more traditional static approach. The uncertainty of the latter is estimated by an ensemble of converged simulations describing a large set of stationary points. The treatment of interconversions between rotational isomers, that is largely overlooked in simulations in the literature, appeared to be key for the accurate determination of pathways and free energies: we propose here a rigorous treatment of this problem. We then reach, with aid of ab initio molecular dynamics, a quantification of the intrinsic free energy barriers and an atomistic explanation of the difference between type A and type B isomerization kinetics.

## 2. METHODOLOGY

### 2.1 Total energy calculations

Periodic DFT calculations were performed using the VASP code [49,50]. The Kohn-Sham equations have been solved variationally in a plane-wave basis set using the projector

augmented-wave (PAW) method of Blöchl [51], as adapted by Kresse and Joubert [52]. The PBE exchange-correlation functional in the generalized gradient approximation proposed by Perdew et al. [53] was used. The D2 correction of Grimme [54] has been applied to account for long-range dispersion interactions that are not treated correctly by local and semilocal density-functional theory. Despite its simplicity, this approach has been shown [55] to improve predictions on structure, energetics, and elastic properties of wide range of materials where dispersion forces play an important role. The PBE+D2 method was also shown to predict reasonable adsorption energies for some of the zeolite-related applications [56]. As a relatively large supercell was employed in calculations (*vide infra*), the Brillouin zone sampling was restricted to the Γ-point. A plane-wave cutoff energy of 400 eV was used in all calculations and the convergence criterion for the electronic self-consistency cycle was set to $10^{-7}$ eV. In the simulations of cations in the gas phase, the charge neutrality of the simulation cell has been preserved by using a compensating uniform background charge.

### 2.2 Transition state search through the static approach

In order to ensure that the reactant, transition state, and product configurations obtained in atomic relaxations discussed in Sections 3.1 and 3.2 are linked by same reaction coordinate, the following strategy has been applied. In the first step, the first-order saddle point on the potential-energy surface corresponding to the transition state for the reaction of interest was identified using the improved dimer method [57,58]. Subsequently, the intrinsic reaction coordinate [59,60] (IRC) for the forward and backward reaction steps was identified using the damped velocity Verlet algorithm [61]. Next, the terminal points from the IRC calculations were relaxed using a conjugate-gradient algorithm [62]. In all atomic relaxations of minima and saddle points, the structures were considered as relaxed when all forces acting on the atoms were smaller than 0.005 eV/Å. Finally, the vibrational eigenspectrum of relaxed structures has been examined and additional line-minimization calculations along undesired

unstable modes have been performed until the computed eigenspectrum contained a correct number of imaginary vibrational frequencies (i.e. zero for stable structures and one for transition states). All relaxations with fixed internal coordinates and a part of the TS optimizations have been performed using the optimization engine GADGET [63,64].

### 2.3 Molecular dynamics simulations

Born Oppenheimer molecular dynamics simulations (MD) have been performed in the (NVT) ensemble. The temperature was controlled with the Andersen thermostat [65] with a collision frequency per atom of 0.01 $fs^{-1}$. The classical equations of motion were integrated using the leapfrog algorithm with an integration step of 1 fs. The atomic mass of tritium has been chosen for all H atoms in order to avoid possible numerical instabilities due to the use of a relatively large integration step. Free energies have been computed using the simulation protocol described in Ref. [43] In this approach based on the transition state theory [65,66], the free-energy of activation ($\Delta A^{\ddagger}$) is defined as follows:

$$\Delta A^{\ddagger} = \Delta A_{\xi_{ref,R}\to\xi^*} - k_B T \ln\left(\frac{h}{k_B T}\frac{\langle|\dot{\xi}^*|\rangle}{2}P(\xi_{ref,R})g_R\right), \qquad (1)$$

where $\Delta A_{\xi_{ref,R}\to\xi^*}$ is the reversible work needed to shift the value of reaction coordinate ($\xi$) from some arbitrary reference value characteristic for reactant ($\xi_{ref,R}$) to the value $\xi^*$ defining the free-energy transition state, $\langle|\dot{\xi}^*|\rangle$ is the average absolute value of velocity of reaction coordinate at the transition state, $P(\xi_{ref,R}) = \langle\delta(\xi - \xi_{ref})\rangle_R$ is the probability density of the state $\xi_{ref,R}$ in ensemble of all reactant (R) configurations, and $g_R$ is the number of symmetry equivalent choices of $\xi_{ref,R}$ corresponding each to a different stable isomer of reactant. As in Ref. [43], the term $\Delta A_{\xi_{ref,R}\to\xi^*}$ is obtained from the blue moon ensemble method (BM) [67,68] implemented in VASP [69], $P(\xi_{ref,R})$ is determined using the straightforward MD simulations, and $\langle|\dot{\xi}^*|\rangle$ is computed numerically using a constrained MD with $\xi(r) = \xi^*$. Free energies of reaction ($\Delta A_{R\to P}$) are computed similarly:

$$\Delta A_{R\to P} = \Delta A_{\xi_{ref,R}\to\xi_{ref,P}} - k_B T \ln\left(\frac{g_R P(\xi_{ref,R})}{g_P P(\xi_{ref,P})}\right). \quad (2)$$

In Equation (2), $\Delta A_{\xi_{ref,R}\to\xi_{ref,P}}$ is the reversible work needed to shift the value $\xi$ from $\xi_{ref,R}$ to some arbitrary reference value $\xi_{ref,P}$ characteristic for product (P), $P(\xi_{ref,P})$ is the probability density of the state $\xi_{ref,P}$ which is, similarly to $P(\xi_{ref,R})$, determined using straightforward MD of the product state, and $g_P$ is the number of symmetry equivalent choices of $\xi_{ref,P}$ corresponding each to a different stable isomer of product. We emphasize that the free energies computed using Equations 1 and 2 are independent of the particular choice of the approximation to the reaction coordinate, provided the approximation drives the transformation from reactant to product reversibly. This property is particularly important when comparing the free energetics of chemical reactions differing in reaction mechanisms and consequently also in definitions of $\xi$. Our method is very closely related to the Bennett-Chandler approach, which is by design invariant with the CV choice [43,65,66]. One can see from equations 1 and 2 or related rate and equilibrium constants expressions [43,65] that all these quantities have correct dimensions independent of the CV choice.

Details of calculations of individual terms of Equations 1 and 2 as well as the corresponding numerical values are presented in Sections SI and SII. The length of straightforward MD simulations used to determine probability densities of reference states was at least 100 ps (see Table S.1) while the length of all constrained MD runs performed with the BM simulations was 50 ps. In each MD run, the initial period of 5 ps has been considered as equilibration and the corresponding data were not used in calculations of ensemble averages. Undesired by-reactions, such as the deprotonation of the reactant or product molecules, have been prevented by the use of restraining potentials described in Section SIII.

A slow growth simulation protocol [70] (MD in which a candidate CV is increased at a constant rate) has been employed in a qualitative way to make sure that the candidate CV can indeed drive smoothly the reaction of interest – from the reactant to the product state, as illustrated in Supporting Information SIV. Our choice of the approximation of reaction coordinate (CV) was validated in a number of internal tests (Supporting Information SIV).

**2.4 Structural Model**

A primitive rhombohedral cell of purely siliceous chabazite (CHA framework, symmetry group R $\overline{3}$ m), with 12 symmetry equivalent tetrahedral sites, was obtained from International Zeolite Association (IZA) database [71]. The cell was optimized (with a cutoff energy of 800 eV) and the resulting lattice constants $a$ =9.336 Å and $\alpha$ = 94.6° are found to be in a good agreement with the experimental reference values [71] ($a$ = 9.304 Å and $\alpha$ = 94.6°). The relaxed structure was subsequently used to build a supercell defined by the lattice vectors $\mathbf{a}_1'$, $\mathbf{a}_2'$, and $\mathbf{a}_3'$ related to the primitive cell vectors of rhombohedral lattice ($\mathbf{a}_1, \mathbf{a}_2, \mathbf{a}_3$) via the following transformations: $\mathbf{a}_1' = \mathbf{a}_2 + \mathbf{a}_3$, $\mathbf{a}_2' = \mathbf{a}_1 + \mathbf{a}_3$, and $\mathbf{a}_3' = \mathbf{a}_1 + \mathbf{a}_2$ (Figure 2). The shortest interatomic separation between the atoms in hydrocarbon and the atoms in its periodically repeated images was not shorter than 5.5 Å. We note that for the sake of consistency, the same supercell has been used also in the gas phase simulations. One of the Si atoms (which are all symmetry equivalent) has been substituted by an Al atom introducing thus a negative charge into the zeolite framework. This negative charge can be formally compensated by attaching a proton onto a framework oxygen atom creating thus a Brønsted acid site (BAS). In this work, however, we investigate reactions in which cationic molecular species occur at all stages whereby the positive charge of cations originates from the proton transferred from the BAS to a neutral molecule. For this reason, no particular Brønsted acid site needs to be considered.

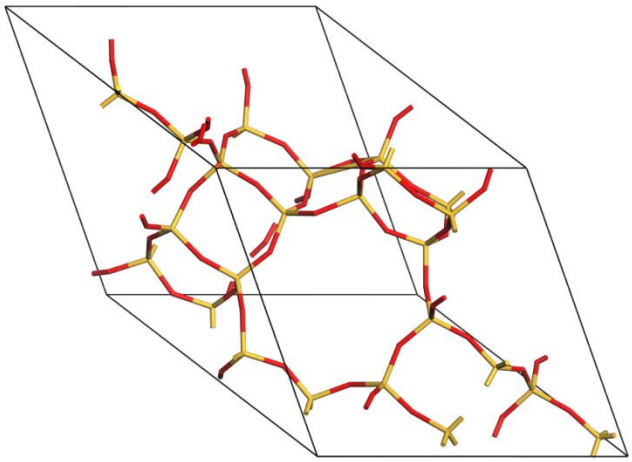

**Figure 2.** Supercell of chabazite used in simulations. (Si in yellow and O in red).

## 3. RESULTS AND DISCUSSION

### 3.1. Isomerization mechanisms and question of the reactant / product rotamers: static approach applied to gas phase reactions

We start by analyzing isomerization reactions of type B and A occurring in the gas phase, which represents the simplest realization of both reactions. The results presented here will be used as reference data for more complicated reactions occurring in zeolite (Sections 3.2, 3.3 and 3.4). Note that all stationary states have been obtained using unconstrained relaxations with very stringent relaxation criteria. A particular attention has been paid to ensure correctness of corresponding eigenvalue spectra. Thus all the stationary states representing reactants and products are all correct unconstrained potential energy minima.

The reactant molecule for type B isomerization (2,4-dimethyl-pent-2-enium cation) forms four stable rotational isomers (rotamers) that can be distinguished by measuring the torsional angle $H^a$-$C^4$-$C^3$-$C^2$ ($\tau$): R(I) with $\tau = 180$ deg., R(III) with $\tau = 0$ deg., and two symmetry equivalent rotamers R(II) with $\tau = \pm 59.1$ deg. The structure of stable rotamers and the numbering of atoms are shown in Figure 3. Potential energy as a function of $\tau$ obtained in a series of constrained relaxations is shown in Figure 4. As evident, the most

stable rotamer R(II) is 3.4 kJ/mol and 1.1 kJ/mol lower in potential energy compared to the cations R(I) and R(III), respectively. Importantly, however, only the conformation of rotamer R(I) is such that type B isomerization is sterically allowed (see below). Indeed, the hydrogen atom $H^a$ is transferred from $C^4$ to $C^3$, while the $C^2$-$C^4$ bond is formed and the $C^3$-$C^4$ bond is broken in the course of this reaction (Figure 1 and Figure 3). Hence the first step of reaction is a transformation of a generic reactant molecule being in any of its stable rotational isomers into the rotamer R(I). As shown in Figure 4, the potential energy barriers for the transformations R(II) →R(I) and R(II) →R(III) (18.7 kJ/mol and 4.6 kJ/mol, respectively) are relatively small compared to the reaction barrier for type B isomerization (*vide infra*). It is therefore reasonable to expect that all rotamers are always at equilibrium with one another and the probability to find the state R(I) at the fixed temperature, volume, and number of particles (NVT ensemble) is given by the Boltzmann distribution law:

$$p\big(R(I)\big) = \frac{e^{-A(R(I))/k_BT}}{e^{-A(R(I))/k_BT} + 2e^{-A(R(II))/k_BT} + e^{-A(R(III))/k_BT}}, \qquad (3)$$

where $A(i)$ is the Helmhotz free energy of the state $i$ and the factor 2 in the denominator reflects the two-fold degeneracy of the state $R(II)$. Using the usual harmonic oscillator and rigid rotor approximation (hereafter termed as static approach), we obtained the values of 4.6 % and 7.5 % for the term $p\big(R(I)\big)$ at T=300 K and 500 K, respectively. As discussed below, the term $p\big(R(I)\big)$ contributes to the free energy of activation.

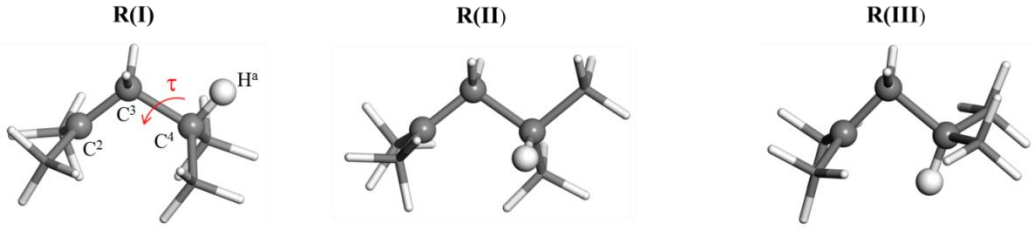

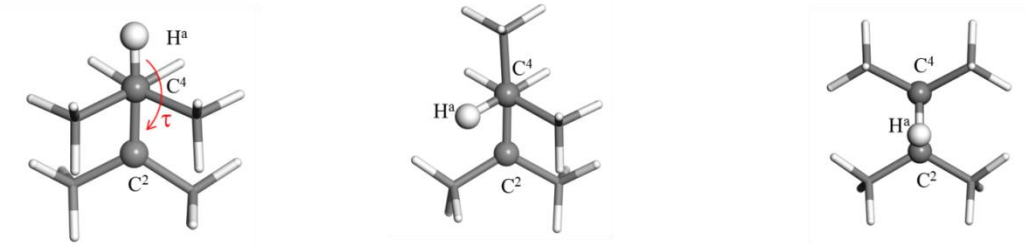


**Figure 3**. Rotational isomers R(I) (τ = 180 deg.), R(II) (|τ| = 59.1 deg) and R(III) (τ = 0 deg.) of the reactant 2,4-dimethyl-pent-2-enium cation. Top panel: side view; bottom panels: front view chosen so that the atom C4 overlaps the atom C3.

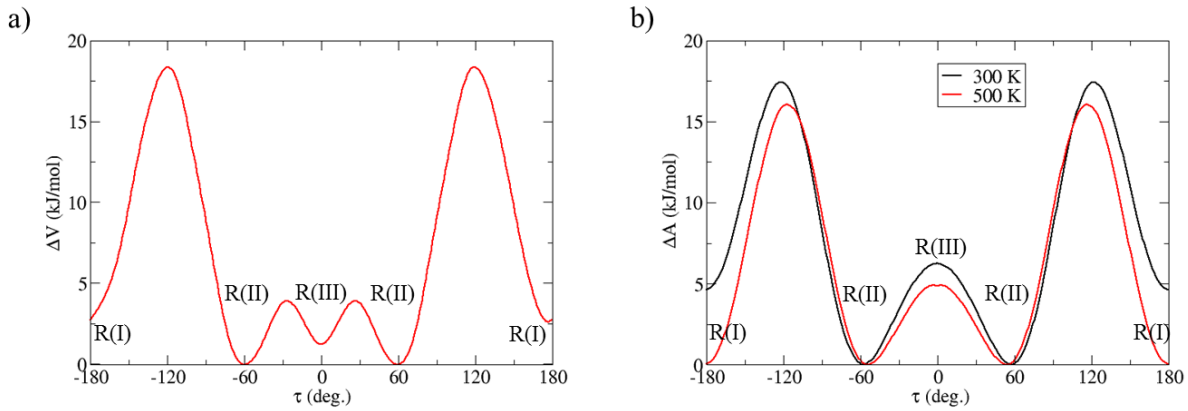


**Figure 4.** a) Potential energy profile along dihedral angle τ computed for the 2,4-dimethyl-pent-2-enium cation in the gas phase at T=0 K, and b) free energy profile computed using MD for the same molecule in chabazite at 300 K and 500 K.

The transition state for type B isomerization ($TS_B$) in the gas phase was identified by the static approach and its structure is shown in Figure 1-a. $TS_B$ is an edge-protonated PCP. In $TS_B$, the two pairs of methyl groups connected to $C^2$ and $C^4$ are face-to-face. By the IRC approach (see movie in supporting information), we show that $TS_B$ is connected to the R(I) rotamer, in which these methyl groups are in the same conformation. Starting from another rotamer (Figure 3) necessary needs to rotate first to generate R(I) then $TS_B$ that are connected. The computed electronic activation energy $\Delta A_{el,R(I)\rightarrow TS_B}$ equals 70.4 kJ/mol. The

free-energy barrier for type B isomerization in the gas phase defined with respect to a generic reactant state R, consisting of all rotational isomers distributed according to the Boltzmann law, can be computed using the formula:

$$\Delta A_{R\rightarrow TS_B} = \Delta A_{R(I)\rightarrow TS_B} - k_B T ln\big(p(R(I))g_{R(I)}\big), \quad (4)$$

where the term $\Delta A_{R(I)\rightarrow TS_B} = A(TS_B) - A\big(R(I)\big)$, which we designate hereafter as the microprocess barrier, corresponds to the free energy of activation for the reaction starting from the active rotamer R(I), whereas the last term on the right hand side is the correction reflecting the fact that the state R(I) is only one of four possible reactant states. As the state R(I) is non-degenerate, the degeneracy factor $g_{R(I)}$ equals unity. The free energy barrier computed using the static approach $\Delta A_{R\rightarrow TS_B}$ increases with temperature as follows: 84.5 kJ/mol (300 K), and 93.4 kJ/mol (500 K). Similarly, the microprocess barriers ($\Delta A_{R(I)\rightarrow TS_B}$) computed for T=300 K, and 500 K are 76.8 kJ/mol, and 82.7 kJ/mol, respectively (see Figure 6). Clearly, the correction term $-k_B T ln(p(R(I)))$ is always positive leading to an increase of free-energy barrier. Furthermore, its contribution (of the order of 10 kJ/mol) increases with increasing temperature, which is obvious from the explicit presence of T in this term (the much weaker implicit dependence introduced via equation (3) tends to decrease $\Delta A_{R(I)\rightarrow TS_B}$ with increasing T). As shown by Tables S2 and S3, the rise of the microprocess barrier with T is mainly due to the entropic term $-T\Delta S_{R(I)\rightarrow TS_B}$ (in particular its vibrational component), which increases by 7.6 kJ/mol when T is changed from 300 K to 500 K, whereas the internal energy of activation changes only by -1.6 kJ/mol at the same temperature interval. The relatively large negative vibrational entropy of activation follows from the loose reactant and tight transition state picture: compared to the reactant, two new bonds ($C^2$-$C^4$ and $C^3$-$H^a$) are being formed while the bonds $C^3$-$C^4$ and $C^4$-$H^a$ present also in the reactant are not yet completely broken in $TS_B$, and hence the PCP transition state structure is geometrically more constrained than the structure of reactant (Figure 1).

The reaction product, the 2,3,3-trimethyl-but-2-enium cation, forms six symmetry equivalent rotational isomers (see Figure S12) separated by a potential energy barrier of 3.0 kJ/mol. The free-energy of reaction R→P writes:

$$\Delta A_{R\to P} = \Delta A_{R(I)\to P(i)} - k_B T ln\left(\frac{p\big(R(I)\big)g_{R(I)}}{p\big(P(i)\big)g_{P(i)}}\right). \quad (5)$$

Similar to Equation (4), the term $\Delta A_{R(I)\to P(i)} = A\big(P(i)\big) - A(R(I))$ is the free energy difference between the particular product and reactant configurations *P(i)* and *R(I)*, whereas the last term accounts for the fact that these states are formed with a certain likelihood among all possible product and reactant configurations. We note that the contributions of $p\big(P(i)\big)$ and $g_{P(i)}$ to Equation 5 cancel each other because all rotational isomers of the product states are symmetry equivalent and hence $p\big(P(i)\big) = \frac{1}{g_{P(i)}}$. The computed potential energy for the product cation is 4.4 kJ/mol lower than that of the configuration R(I) and the term $\Delta A_{R(I)\to P(i)}$ varies with T as follows: -4.9 kJ/mol (300 K), and -5.0 kJ/mol (500 K). The sign and magnitude of $\Delta A_{R(I)\to P(i)}$ are almost fully determined by the internal energy of reaction (Table S3), whereas the entropy of reaction is negligible (the computed values of $-T\Delta S_{R(I)\to P(i)}$ are 0.0 kJ/mol at 300 K and 0.6 kJ/mol at 500 K). Taking the configurational term $-k_B T ln(p(R(I)))$ into account, both the sign and the value of $\Delta A_{R\to P}$ change (2.8 kJ/mol (300 K) and 5.8 kJ/mol (500 K)).

The product of type B isomerization can further undergo type A isomerization reaction. The product of the latter reaction is, in the case considered in this work, chemically identical to the reactant (i.e. 2,3,3-trimethyl-but-2-enium cation), hence the free energy, internal energy, and entropy of reaction are zero by definition. Unlike type B isomerization, the free energy barrier $\Delta A_{P(i)\to TS_A}$ depends weakly on T (see Table S4), the computed values are 14.7 kJ/mol (300 K), and 16.2 kJ/mol (500 K) (see Figure 6). In this case, the effect of newly formed bond $C^3$-$C^4$ in transition state ($TS_A$) is compensated by a significant weakening

of the $C^2$-$C^3$ bond, which is elongated to the same length as the newly formed $C^3$-$C^4$ (1.84 Å). $TS_A$ is a corner-protonated PCP. Hence the structure of the PCP ring in TSA is not more strongly constrained than the reactant configuration and the tight reactant and loose transition state picture valid for type B isomerization does not apply to type A isomerization. This result explains why the computed entropy of activation takes a relatively small value (the computed values of $-T\Delta S_{P(i)\rightarrow TS_A}$ are 1.8 kJ/mol and 4.7 kJ/mol for T=300 K and 500 K, respectively). As all rotamers formed by the reactant (or product) molecule are equivalent by symmetry, the last term in the formula $\Delta A_{P\rightarrow TS_A} = \Delta A_{P(i)\rightarrow TS_A} - k_B T ln\big(p(P(i))g_{P(i)}\big)$ is zero due to cancellation of terms $p(P(i)$ and $g_{P(i)}$ and hence the free energy of activation is identical to the microprocess free energy barrier.

### 3.2. Static approach applied to reactions in zeolite

Within a zeolite framework, the mechanisms of both isomerization reactions remain the same as in the gas-phase because the atoms of the zeolite framework are not covalently bonded to the intermediates involved. Nevertheless, the electrostatic interaction and dispersion forces between the zeolite and the molecule increase tremendously the complexity of the potential energy surface (PES), which now contains many local stationary points corresponding to structures differing in the orientation and the relative position of the molecule with respect to the zeolite internal surface at each step of the reaction. In this section, we demonstrate that the increased complexity of PES introduces an unacceptably large and hard to control error into the calculations of reaction free-energetics determined via the static approach.

To this end, a set of seven TS configurations has been determined by means of geometric relaxations for both chemical reactions considered in this work, whereby the initial configurations (used for the relaxations) have been obtained from constrained molecular

dynamics simulations described in Sections 3.3.3 and 3.4.3. In all cases, $TS_A$ and $TS_B$ remain corner and edge-protonated PCPs respectively (see also later, a detailed structural analysis in sections 3.3.4 and 3.4.4.). We emphasize that our sets of TS configurations are by no means exhaustive – they have been chosen only to highlight the strong limitation of the static approach applied to such complex systems. Upon determining the TS configurations, the reactant and product configurations have been obtained by means of the IRC analysis (see Section 2). The vibrational spectra of all relaxed configurations were carefully checked to ensure that all relaxed structures were correct stationary points of PES.

As shown in Table S5, the potential energies of optimized TS structures for type B isomerization are spread over a very broad range of values, the difference between the highest and the lowest TS energies being as large as 40.2 kJ/mol. This large variation in energy is due to significant differences in the TS orientation and position within the zeolite framework whereas the molecular structure of each TS is rather similar (Table S8). As shown in Figure S13, the potential energy of individual TS configurations correlates rather well with the parameter $\chi$ defined as

$$\chi = \sum_{i=1}^{N_C} \frac{1}{[d(Al - C^i)]^6} \qquad (6)$$

where $d(Al - C^i)$ is the distance between aluminum atom and the carbon atom $i$, and the sum is over all carbon atoms in the system ($N_C$). Taking into account that the framework Al is surrounded by four oxygen atoms with increased negative charge and some of the C atoms bears a partial positive charge, we deduce that the variation of the potential energy of individual TS configurations is mainly attributed to the electrostatic and dispersion interactions between the PCP and the zeolitic framework. The distance $C^4$–Al in relaxed TS structures, for instance, varies from 3.88 Å to 5.96 Å (the two extreme cases are shown in Figure 5 while all TS structures are shown in Figure S14 and the corresponding data are

given in Table S8) indicating that the PCP can be stabilized in many different places of the zeolite micropores.

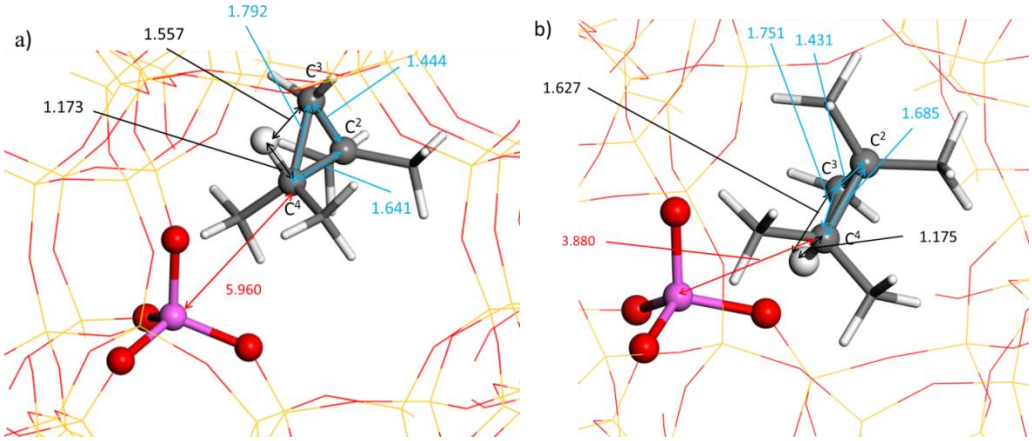


**Figure 5.** Selected transition state configurations for type B isomerization: relaxed structure with the longest (a) and the shortest (b) separation between atoms $C^4$ and Al. (Al in purple, H in white, Si in yellow and O in red). Selected interatomic distances are in Å.

The variation of vibrational contribution to free energy of $TS_B$ resulting from differences in the low-frequency part of the vibrational spectra (Table S5) are as large as 13.6 kJ/mol (300 K) and 22.6 kJ/mol (500 K). The variation in the total free energy of $TS_B$ configurations is ~40 kJ/mol for both temperatures considered in this work (Table S5), which is very similar to the variation in the potential energy reported above.

Results obtained for type A isomerization (Table S11) show that the variation of potential energy for the relaxed $TS_A$ structures spreads over a narrower interval of width of 11.1 kJ/mol (Table S9). As in the case of $TS_B$, the electronic energy of the $TS_A$ structures identified in this work correlates rather well with the parameter $\chi$ defined above (see Figure S13), albeit the spread of the $\chi$ values is much narrower. The latter fact indicates that the variation of orientations and positions of $TS_A$ sampled in our static calculations is much smaller than that for the $TS_B$ configurations. The maximal and minimal vibrational free-

energy determined for the TS structures at 300 K and 500 K differ by 13.3 kJ/mol and 20.7 kJ/mol, respectively. The resulting variation in the total free energy of $TS_A$ is 11.8 kJ/mol and 17.4 kJ/mol for T=300 K and 500 K, respectively. Once again, the intramolecular structures of all relaxed reactant and product configurations are found to be rather similar to their gas-phase counterparts (see Figure S15 for the first two configurations and the Table S12 with geometric data of the PCPs) and the variation in the computed potential energy stems almost exclusively from the differences in the position and orientation of the molecule in the zeolite.

All these results have important practical consequence: if only a single static calculation is performed to explore a chemical reaction similar to those studied in this work, as it is often the case in the literature, the uncertainty in the computed free energy of $TS_A$ is of order of 10 kJ/mol (40 kJ/mol for $TS_B$) and it increases with T.

In practice, however, one is usually interested in relative (e.g. free energies of reaction and activation) rather than in absolute free energies of a given state. Hence the important question is to which extent the above-mentioned uncertainty is reflected into the uncertainty in computed free-energy barriers. In order to address it, the reactant and product configurations linked with the different TS configurations have been determined by means of IRC analysis. The contributions to the total free energies are reported in Tables S7 and S11, and illustrated in Figure 6 for type B and type A isomerization reactions at T=300K. The uncertainty in computed free energy differences is enormous.

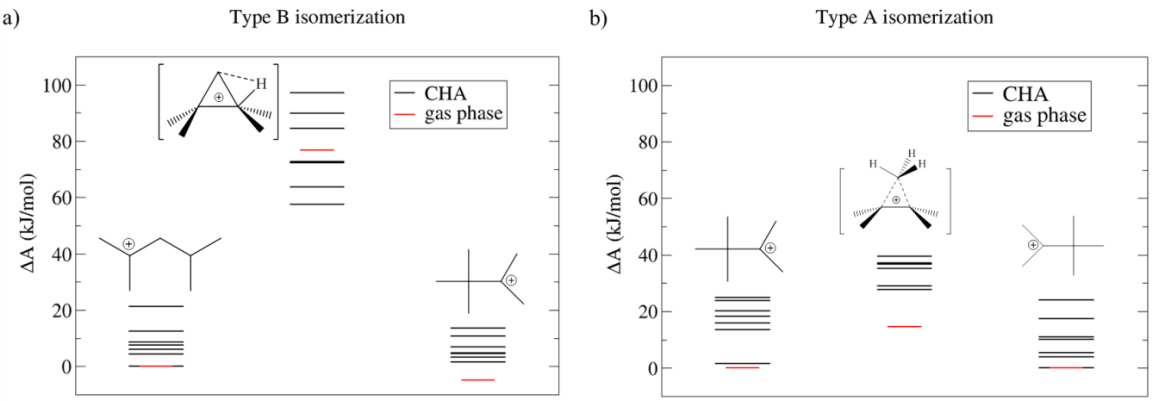


401

402 **Figure 6.** Distribution of free energy values computed in seven independent simulations based on
403 static approach for the microprocess transformation of a) type B and b) type A isomerization reactions
404 in chabazite at T = 300 K . For both reactions, the lowest energy of reactant states defines zero on the
405 free energy scale. For the sake of comparison, the values computed for the reactions in gas phase are
406 also shown.

407

408 Depending on the transition state, the microprocess barrier $\Delta A_{R(I)\rightarrow TS_B}$ for the forward
409 mode of type B isomerization ranges between 50.1 kJ/mol to 84.5 kJ/mol at 300 K (76.8
410 kJ/mol in gas phase, Figure 6) and between 52.5 kJ/mol to 85.7 kJ/mol at 500 K (82.7 kJ/mol
411 in gas phase), respectively (Table S7). The variation in the microprocess barrier for the
412 reverse mode is similar: 46.8 kJ/mol to 92.6 kJ/mol at 300 K (81.7 kJ/mol in gas phase) and
413 49.5 kJ/mol to 94.0 kJ/mol at 500 K (87.7 kJ/mol in gas phase). The microprocess barrier for
414 type A isomerization varies between 8.7 kJ/mol to 37.2 kJ/mol at 300 K and 5.1 kJ/mol to
415 42.6 kJ/mol at 500 K, respectively (Table S11). As mentioned in Section 3.1, the reactant and
416 product states of type A isomerization studied in this work are chemically identical, and
417 hence the forward and reverse reaction modes are indistinguishable.

418 Finally, we point out that the uncertainty in free energy of activation increases further if
419 one does not ensure that all stationary states of reaction are linked by a common IRC, as it is

unfortunately often the case in the literature. On basis of our results we estimate that in the most extreme case, the microprocess barrier for the forward reaction mode of type B isomerization at 300 K, for instance, can spread over the interval between 36.4 kJ/mol to 97.2 kJ/mol if the reactant and TS configurations are determined in two independent static calculations.

Altogether, we have shown that the use of the static approach to study isomerization reactions in zeolites is highly problematic. Clearly, in order to overcome the limitations of this approach, one has to efficiently sample the configuration space relevant for the reaction of interest. As we shall discuss in Sections 3.3 and 3.4, this task can be elegantly accomplished by means of molecular dynamics.

### 3.3. Molecular Dynamics of type B isomerization in zeolite

#### 3.3.1. Choice of the approximation to the reaction coordinate

The MD method used in this study to determine the free energy of activation (Section 2.3) requires the use of a suitable approximation of the reaction coordinate ($\xi$), which must be able to reversibly drive the reaction from its initial to the final state. For this purpose, we used a path-based collective variable ($\xi$) introduced by Branduardi et al. [72], which is defined as follows:

$$\xi = \frac{1}{M-1}\frac{\sum_{i=1}^{M}(i-1)exp(-\lambda|\boldsymbol{q}-\tilde{\boldsymbol{q}}(i)|^2)}{\sum_{i=1}^{M}exp(-\lambda|\boldsymbol{q}-\tilde{\boldsymbol{q}}(i)|^2)}, \quad (7)$$

where $\boldsymbol{q}$ is a multidimensional vector whose components are primitive coordinates describing the changes in the structure of the system during the reaction, $\tilde{\boldsymbol{q}}(i)$ is the position vector (defined in the same primitive coordinate space as $\boldsymbol{q}$) of the $i$-th point of a discretized reaction path $\{\tilde{\boldsymbol{q}}(i); i = 1, \dots, M\}$, $M$ is the total number of points in $\{\tilde{\boldsymbol{q}}(i)\}$, and $\lambda$ is an adjustable parameter. The neighboring points of $\{\tilde{\boldsymbol{q}}(i)\}$ should be approximately equidistant

and the parameter $\lambda$ should be chosen so as to correspond to the average value of $|\widetilde{\boldsymbol{q}}(i) - \widetilde{\boldsymbol{q}}(i+1)|^2$ [72,73]. By construction, the value of $\xi$ ranges between 0 (reactant) and 1 (product).

As shown in Sections 3.1 and 3.2, the activation energy of type A isomerization is relatively small and hence this reaction can occur spontaneously during the MD simulations of the product configurations of type B isomerization. In order to prevent this undesired process, the coordinate $\xi$ has been defined so as to cover both subsequent isomerization reactions. To this end, the following lengths of the carbon-carbon and carbon-hydrogen bonds involved in type B and A isomerization reactions have been chosen as the primitive coordinates defining $\widetilde{\boldsymbol{q}}$ and $\boldsymbol{q}$: $C^2$-$C^3$, $C^3$-$C^4$, $C^2$-$C^4$, $C^4$-$H^a$, and $C^3$-$H^a$ (Figure 3). We note that this choice has been made with type B isomerization in mind and it is not optimal for type A isomerization where the atom $H^a$ plays no special role. The reaction coordinates for both reactions have been approximated by the corresponding IRC determined for the gas-phase reaction discussed in Section 3.1 and merged via the common point corresponding to the product of type B isomerization, which is identical to the reactant of type A isomerization (see Section 3.1). The discretized reaction path $\{\widetilde{\boldsymbol{q}}(i)\}$ has been subsequently defined by choosing 20 approximately equidistant points. With this setting, the interval of $\xi$ between 0 and ~0.77 corresponds to type B isomerization while the interval between ~0.77 and 1 covers type A isomerization.

### 3.3.2. Characterization of reactant and product states

As discussed in Section 3.1, out of four rotational isomers of the reactant molecule (2,4-dimethyl-pent-2-enium cation), only the rotamer designated as R(I) can be directly transformed into the transition state for type B isomerization. It is therefore natural to choose a high-likelihood state of the rotamer R(I) as a reference state $\left(\xi_{ref,R}\right)$ for the use in the free energy calculations (Equation 1). A direct calculation of the probability density $P\left(\xi_{ref,R}\right)$ by

the straightforward MD would be extremely inefficient due to the relatively high free energy barriers (as compared to $k_BT$) separating the stable rotational isomers of reactant (Figure 4). In order to circumvent this problem, we express the density of the reference reactant state as follows:

$$P\left(\xi_{ref,R}\right) = \tilde{P}\left(\xi_{ref,R}\right) \times p\left(R(I)\right), \tag{8}$$

where $\tilde{P}\left(\xi_{ref,R}\right) = \langle \delta(\xi - \xi_{ref,R}) \rangle_{R(I)}$ is the probability density of the reference state in the ensemble of all realizations of the state R(I), and $p\left(R(I)\right) = \frac{\int_{q\in R(I)} dqdp\, e^{-\frac{H(q,p)}{k_BT}}}{\int_{q\in R} dqdp\, e^{-\frac{H(q,p)}{k_BT}}}$ is the probability of the state R(I) among all reactants states. The two terms of Equation 8 are computed in two different sets of simulations that we discuss below.

The term $p\left(R(I)\right)$ is obtained from the free energy profile $A(\tau)$ computed using the blue moon ensemble method [67,68] whereby the torsional angle τ is defined in Section 3.1. Altogether 10 integration points evenly distributed over the interval $0 \leq \tau < \pi$ have been used and the full profile A(τ) ($-\pi \leq \tau < \pi$) has been built by employing the symmetry of the molecule dictating the relations $A(-\tau) = A(\tau) = A(\tau + 2\pi)$. As obvious from Figure 4, the finite temperature free energy profiles determined for reactant in chabazite are similar in shape to the zero temperature potential energy profile computed for the reactant in the gas phase. The only qualitative difference is the absence of the shallow minimum at τ=0. As we show in Section SV.1, this interesting variation is caused by the fact that, unlike the isomers R(I) and R(II), the rotamer R(III) (τ=0) is stable only if the skeletal angle C4-C3-C2 ($\alpha$) is below 100 deg. At increased temperature, however, the thermal motion of atoms leads to an increase in average value of $\alpha$ making the isomer R(III) unstable. Apart from this detail, the calculations predicted the expected trends: an increase in temperature leads to a decrease in free energy differences between minima corresponding to the stable rotamers R(I) and R(II), and the barrier for the R(II)→R(I) transformation (transition states positioned at $\tau_{max,1} \approx$

$-120°$ and $\tau_{max,2} \approx 120°$) decreases with increasing T. The probability of the state R(I) among all reactant configurations, computed using the formula $p\big(R(I)\big) = \frac{\int_{\tau_{max,1}}^{\tau_{max,2}} exp\left(-\frac{A(\tau)}{k_B T}\right) d\tau}{\int_{-\pi}^{\pi} exp\left(-\frac{A(\tau)}{k_B T}\right) d\tau}$, therefore increases from 6.4 % at T=300 K to 27.9 % at 500 K. We note that while the former value is similar to that determined using the static approach for the cation in gas phase (4.6 %), the latter is significantly greater than its static approach gas phase counterpart (7.5 %).

Probability density $\tilde{P}\big(\xi_{ref,R}\big)$ is determined using the straightforward MD of the state R(I). For both simulation temperatures considered in this work, the free energy barriers separating the rotamers R(I) and R(II) are relatively high compared to the $k_B T$ term, which ensures that the transformation R(I)→ R(II) is a slow process occurring only very infrequently on the time scale of our MD simulations. The probability densities computed for T=300 K and 500 K are shown in Section SI. The values determined for the reference state $\xi_{ref,R} = 0.069$ are 23.5 (300 K) and 16.3 (500 K). Finally, we determine the following values of $P\big(\xi_{ref,R}\big)$ using equation 8: 1.5 (300 K) and 4.5 (500 K).

A similar analysis has been performed also for the product state (2,3,3-trimethyl-but-2-enium cation formed in chabazite). In this case, the calculation was simplified by the fact that all six stable rotational isomers of the product state are equivalent by symmetry (see Section 3.1), and hence the following equality holds: $g_P P\big(\xi_{ref,P}\big) = \langle \delta(\xi - \xi_{ref,P}) \rangle_{P(i)}$. Choosing the reference state $\xi_{ref,P} = 0.769$, the calculations based on the straightforward MD performed for the product state led to the following values of $g_P P\big(\xi_{ref,P}\big)$: 17.9 (300 K) and 14.9 (500 K).

### 3.3.3. Free energy calculations

In order to determine the terms $\Delta A_{\xi_{ref,R} \to \xi^*}$ and $\Delta A_{\xi_{ref,R} \to \xi_{ref,P}}$ used in calculations of free energies of activation and reaction (see Section 2.3), blue moon ensemble approach [67,68]

has been employed. To this end a mesh of 16 integration points has been used corresponding to states distributed between the reference reactant ($\xi_{ref,R}$) and product ($\xi_{ref,P}$) states defined in Section 3.3.2. The free energy profiles $A(\xi)$ computed for T=300 K and 500 K are shown in Figure 7. The free energy transition state ($\xi^* \approx 0.338$) has been identified as the maximum on $A(\xi)$ and the values of the velocity term $\left|\dot{\xi}^*\right|$ ($1.75 \cdot 10^{12}$ $s^{-1}$ and $2.29 \cdot 10^{12}$ $s^{-1}$ for T=300 K and 500 K, respectively) have been determined as described in Section SII. The computed contributions of the term $\Delta A_{\xi_{ref,R} \to \xi^*} = A(\xi^*) - A(\xi_{ref,R})$ to the free energies of activation at 300 K and 500 K are 70.5 (± 3.4) kJ/mol and 80.5 (± 3.6) kJ/mol, respectively (taking into account the standard error on the mean values of the gradients of the free energy, for a confidence interval of 95%). Employing equation 1 along with the data presented in Section 3.3.2, the free energies of activation of 74.4 (± 3.4) kJ/mol and 83.4 (± 3.6) kJ/mol have been obtained for T=300 K and 500 K, respectively. These values are ~10 kJ/mol lower than those computed using the simple static approach for the reaction in the gas phase discussed in Section 3.2. Such a difference is not unexpected as the latter simulations use a more approximate physical model and completely neglect the interactions between the molecule and zeolite. In this light it is remarkable that both sets of simulations predict almost the same change in the free energy of activation (~9 kJ/mol) due to the increase of T from 300 K to 500 K. This result suggests that the temperature trend in activation energy of this monomolecular reaction is entirely determined by entropy related to the intramolecular vibrations while the contribution of those degrees of freedom related to interactions with zeolite is negligible. This conclusion is even underlined by the similarity in average geometry of transition states identified in MD with the zero temperature TS geometry for the gas phase reaction (see Section 3.3.4), which is consistent with the tight TS and loose reactant picture.

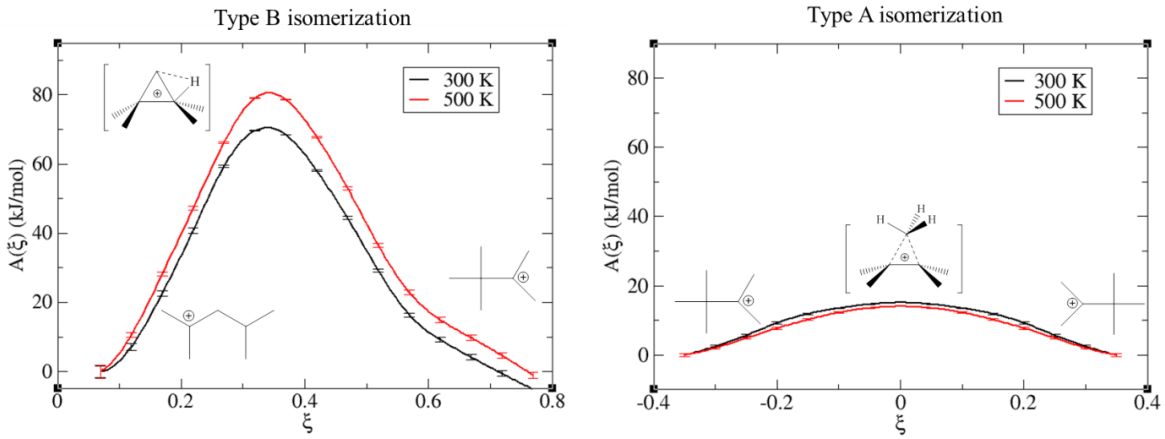


**Figure 7.** Free energy profiles ($A(\xi)$) computed using the bluemoon ensemble approach for type B (left) and type A (right) isomerization reactions in chabazite at T=300 K and 500 K. The error bars are determined from the standard errors on the free energy gradients [69].

The free energies of reaction computed using Equation (2) for T=300 K and 500 K are 1.9 (± 3.8) kJ/mol and 3.7 (± 4.2) kJ/mol, respectively. These results are, again, in qualitative agreement with predictions made on the basis of the simple static approach for the reaction in the gas phase predicting a negligible change in the free energy of reaction due to the temperature increase from 300 K to 500 K (see Section 3.1).

### 3.3.4 Structural analysis of $TS_B$ at finite temperature

**a) C-C and C-H bonds**

The distribution of the C-C and C-H bonds in the PCP obtained in the MD runs are reported in Figure 8. The C-C and C-H bonds in the $TS_B$ are typical for the constrained edge protonated cyclopropane and their averages are very similar to the values found for $TS_B$ in the gas phase reaction determined in the static approach (see Section SVII).

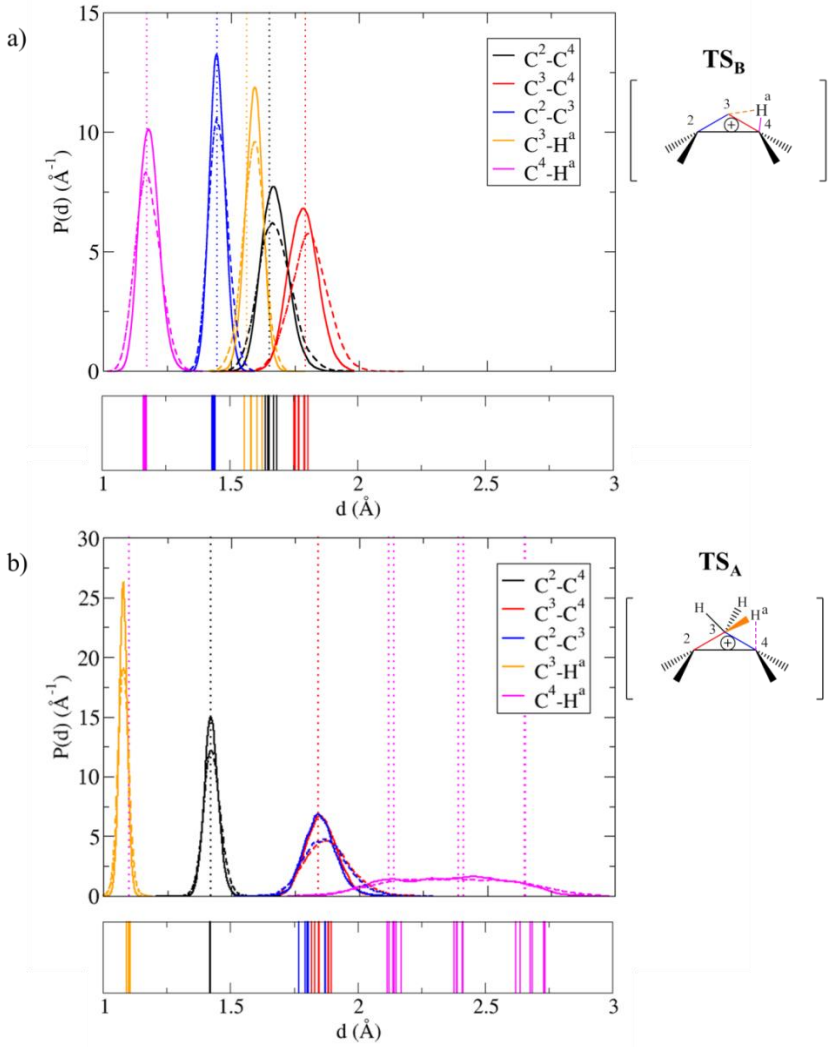


**Figure 8.** Probability distributions of selected C-C and C-H bond lengths in the transition states of (a) type B isomerization ($TS_B$), and (b) for type A isomerization ($TS_A$) determined using MD at 300 K (solid lines) and 500 K (dashed lines). For the sake of comparison, the static approach results for the gas phase reactions are also indicated by vertical dotted lines. Bottom panels show data determined for the series of static calculations for reactions in chabazite discussed in Section 3.2.

Furthermore, the relation between the standard deviation of the bond length distribution and its effective force constant [74] allows us to conclude that the bond $C^2$-$C^4$ formed during reaction is stronger in transition state than that in reactant, while the other two bonds involved in the PCP formation ($C^3$-$C^4$ and $C^2$-$C^3$) are comparably strong (see Section SVII.1 and Table

S13) and this result is consistent with the tight TS loose reactant picture. The intramolecular geometry of structures optimized in the zeolite are rather similar to the average MD structures and this agreement indicates that the very large difference in energy and free energy between relaxed structures is not due to intramolecular geometric features.

**b) Location of $TS_B$ with respect to Al**

In Section 3.2 we showed that the electronic energy of transition states correlates with the inverse distances between Al and C atoms (measured via parameter $\chi$), which, in turn reflects the variation in distribution of the molecule within the cavity of zeolite. In the constrained molecular dynamics run of the transition state at 300 K (Figure 9-a), the parameter $\chi$ ranges between 0.0005 $Å^{-6}$ and 0.0017 $Å^{-6}$ and the distribution of $\chi$ is bimodal with maxima at $2.7 \cdot 10^{-4}$ $Å^{-6}$ and $7.0 \cdot 10^{-4}$ $Å^{-6}$.

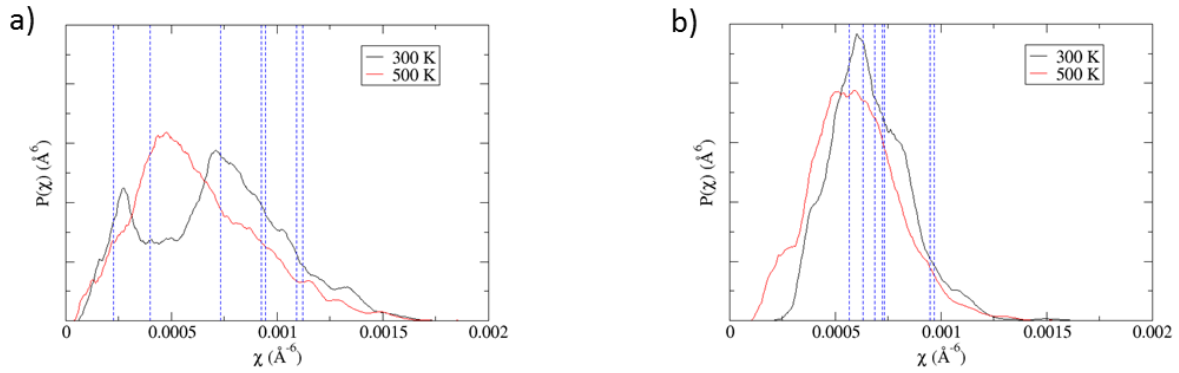


**Figure 9.** Probability distribution of the sum of inverse distances between the framework Al and all C atoms raised to the power of six ($\chi$) determined for the transition state of type B (a) and type A (b) isomerization in chabazite determined using MD at T = 300 K and 500 K. For the sake of comparison, the static approach results for the reaction in chabazite are indicated by vertical dashed lines.

The various $TS_B$ determined in the series of static calculations are located fall into different parts of this distribution. At 500 K, the shape of the distribution changes and the dominant peak is shifted towards longer distances (i.e. smaller $\chi$). Obviously, such an effect cannot be

taken into account using a simple static approach based on the harmonic approximation because the potential energy minimum structure is always the most likely configuration regardless of temperature.

### 3.4. Free energy calculations for type A isomerization reaction

#### 3.4.1. Choice of the approximation to the reaction coordinate

As described in Section 3.3.1, the parameter $\xi$ used in free energy calculations of type B isomerization has been constructed so as to cover also type A isomerization but the only purpose of such a choice was to prevent the uncontrolled transformation of the product configuration. Unfortunately, this approximation of reaction coordinate is not suitable for calculations related to type A isomerization because it involves two C-H distances defined for a specific hydrogen atom ($H^a$) which plays no particular role in this reaction. The undesired consequence is that any rotation of the $CH_3$ group containing $H^a$ would be artificially hindered. In order to avoid such problems, we use for type A isomerization the following approximation of reaction coordinate which is defined only via positions of carbon atoms, and it is invariant with respect to the interchange of $CH_3$ groups attached to the same central carbon atom:

$$\xi = \eta(C^2) - \eta(C^4), \tag{9}$$

where $\eta(C^i)$ is the coordination number [75] of central carbon atom $C^i$ with respect to the carbon atoms $C^1$, $C^3, C^5, C^6$, and $C^7$ (the numbering of atoms is as in Figure 1-b), which we defined as follows:

$$\eta(C^i) = \sum_{j=1,3,5,6,7} \frac{1 - \left(\frac{d(C^i - C^j)}{d_{ref}}\right)^9}{1 - \left(\frac{d(C^i - C^j)}{d_{ref}}\right)^{14}} \tag{10}$$

606 with $d_{ref} = 1.7$ Å being the reference length for the C-C bond. During type A
607 isomerization, the reaction coordinate varies in the interval between –0.4 to 0.4 and $\xi^* = 0$
608 by symmetry.
609
610 **3.4.2. Characterization of reactant and product states**
611 As explained in Section 3.1, the reactant and product of type A isomerization are symmetry
612 equivalent. Because both states are equivalent to the product of type B isomerization, we
613 employ in this section the labeling used in Section 3.3 and designate the reactant/product
614 states of type A isomerization as P. The chosen reference state $\xi_{ref,P} = -0.35$ (see Equation
615 1) corresponds to a high-likelihood state in the free MD runs at both temperatures considered
616 in this study (see Figure S3). As the potential energy barrier for the transformation between
617 the six symmetry equivalent rotational isomers is only 3.0 kJ/mol (see Section 3.1),
618 straightforward MD simulations can be used to determine the probability density of the
619 reference state. The values of $\tilde{P}(\xi_{ref,P}) = g_P P(\xi_{ref,P})$ computed for T=300 K and 500 K are
620 2.45 and 2.25, respectively.
621
622 **3.4.3. Free energy calculations**
623 As in Section 3.3.3, the blue moon ensemble approach [67,68] has been used to determine
624 the term $\Delta A_{\xi_{ref,P} \to \xi_A^*}$. In our calculations, a mesh of eight integration points corresponding to
625 states distributed between the reference reactant ($\xi_{ref,P} = -0.35$) and the transition states
626 ($\xi_A^* = 0$) has been used. The full free energy profiles $A(\xi)$ computed for T=300 K and 500 K
627 (Figure 7) have been subsequently obtained by making use of the symmetry of the problem
628 ($A(-\xi) = A(\xi)$), which follows from the fact that the reactant and the product molecules are
629 symmetry equivalent. The values of the velocity term $|\dot{\xi}^*|$ (5.68 $10^{12}$ $s^{-1}$ and 7.34 $10^{12}$ $s^{-1}$ for
630 T=300 K and 500 K, respectively) have been determined as described in Section SII. The

computed contributions of the term $\Delta A_{\xi_{ref,P}\rightarrow\xi^*} = A(\xi^*) - A(\xi_{ref,P})$ to the free energies of activation of type A isomerization at 300 K and 500 K are 15.1 (± 0.8) kJ/mol and 14.0 (± 0.9) kJ/mol, respectively. Combined with the data presented in Section 3.4.2, the free energies of activation computed using Equation 1 are 14.9 (± 0.8) kJ/mol and 15.0 (± 0.9) kJ/mol for T=300 K and 500 K, respectively. Hence, the free energy of activation for type A isomerization is, according to our simulations, basically independent on temperature, which is in agreement with the conclusion made in Section 3.1, where a simple static approach for the reaction in the gas phase was discussed.

### 3.4.4 Structural analysis of $TS_A$ at finite temperature

**a) C-C and C-H bonds**

The analysis of the distributions of the $C^2$-$C^3$ and $C^3$-$C^4$ bonds shows that they are both significantly looser than the chemical bond $C^2$-$C^4$, which is comparably strong as the C-C bonds in the reactant (see Figure 8-b and Section SVII.2 and Table S13). Moreover, visual inspection of the MD structures reveals that the methyl group shifted during the reaction freely rotates (unlike the $CH_3$ group formed during type B isomerization). This is clearly illustrated in Figure 8-b, where a narrow distribution of the $C^3$-$H^a$ bond centered at a typical bonding distance (~1.1 Å) is found while the distribution for the non-bonding $C^4$-$H^a$ distance is very broad because of rotations of the methyl group shifted during the reaction. This analysis confirms that the transition state for type A isomerization, of corner-protonated PCP nature, is much less constrained than that for type B isomerization, of edge-protonated nature. Altogether, despite the apparent similarity in TS structures of type A and B isomerization reactions (both TS are usually represented by very similar schemes in chemical textbooks), both structures differ in the strength of C-C bonds which are formed or broken, and in the

655 specific role of the H transfer in $TS_B$, which in turn leads to significant differences in free
656 energy of activation and in the thermal dependence of the latter.

657 **b) Location of $TS_A$ with respect to Al**

658 As in the case of type B isomerization, we explore the distribution of the $TS_A$ within the
659 zeolite cavity by analyzing the parameter $\chi$ (see Section 3.2). As shown in Figure 9-b, $\chi$
660 varies between $1.4 \cdot 10^{-4}$ Å$^{-6}$ and $1.4 \cdot 10^{-3}$ Å$^{-6}$ and the distribution shows one dominant
661 maximum which is shifted towards smaller $\chi$ with increased T ($6.1 \cdot 10^{-4}$ Å$^{-6}$ (300 K) and
662 $5.5 \cdot 10^{-4}$ Å$^{-6}$ (500 K)). As evident from Figure 9-b, most of the first order saddle points on the
663 PES determined in our static calculations (see Section 3.2) are located close to the maximum.
664 While our static transition state search identified two configurations corresponding to $TS_A$
665 with significantly larger than average $\chi$ (i.e. with shorter than average effective distances
666 between Al and C atoms), no configuration from the region $\chi < 5 \cdot 10^{-4}$ Å$^{-6}$ has been found (see
667 Figure 9-b). The fact that the latter region is populated mainly at high T points once again at
668 the systematic failure of the naïve static approach to account for non-trivial thermal effects.
669

670 **3.5. On the atomic origin of the different kinetics of type A versus type B isomerization**
671 **reactions in zeolites**

672 Somewhat surprisingly at first sight, the results obtained using the sophisticated and
673 time-consuming MD simulations are in qualitative and even semi-quantitative agreement
674 with the calculations performed using the static approach for the gas phase reactions. Indeed,
675 the latter set of calculations predicted the correct thermal trends for free energies of activation
676 and of reaction for both temperatures, although the numerical values are overestimated by up
677 to 16 %. Such a qualitative agreement is possible because of the following reasons: (i) the
678 effect of interactions of molecule with CHA zeolite on reaction barriers is only modest, and
679 (ii) the approximations used in the static approach are reasonable when applied to relatively

680 small gas phase molecules. The point (i) can be understood because the CHA zeolite does not
681 directly participate in chemical reactions analyzed in this work, and the nature of interaction
682 between the CHA zeolite and the molecule does not change during the chemical reaction.
683 Thus, confinement effect is roughly the same for the reactants, the transition states and the
684 products in the case we are investigating. Note however that shifting from the CHA zeolite
685 (used here) to another framework, or from one kind of channel/cage to another one contained
686 within the same zeolite, the extent of the confinement effect is expected to change [76], likely
687 altering the catalytic performance. In particular, in the case of smaller cages or channels (such
688 as ZSM-22 for example, mono-dimensional 10 MR framework), one may expect a
689 differentiation of the zeolite/cation interactions depending on subtle steric constraint changes,
690 such as the one taking place in the course of the reactant → transition state → product
691 transformation. Similar differentiation may occur in the case of bulkier reactants as compared
692 to the C7 molecules considered here. The point (ii) follows from the fact that the harmonic
693 oscillator model used in the static approach performs rather well when describing vibrations
694 of the intramolecular degrees of freedom [77,78]. Furthermore, the size and shape of the large
695 CHA cavity where the reaction takes place restricts only very weakly the molecular rotations
696 in our case, and this modest restriction is similar for all stages of reaction. Hence also the
697 rotational contribution to free energy differences predicted by the gas phase model is
698 reasonable. Finally, the translational contribution computed using the static approach for a
699 gas phase molecule depends only on the molecular mass and the volume available for the
700 motion [79]. As both of these quantities are constant in the case of the monomolecular
701 reaction at the NVT conditions, the contribution of translational degrees of freedom to the
702 relative free energetics of a monomolecular gas phase reaction must vanish. In the case of
703 reaction in zeolite, the volume available for the translation motion of molecule remains
704 approximately constant during the reaction. Because also the nature of interaction between

the molecule and zeolite remains essentially unaltered, the contribution of translational degrees of freedom also largely vanishes in the MD based calculations of free energy differences for a monomolecular reaction in zeolite. In contrast, an attempt to describe hindered rotations and translations of a molecule in zeolite by harmonic oscillator model, as it is done when using the static approach in zeolite, necessarily fails because of large contribution of low frequency vibrational modes to free energy and because of complexity of underlying potential energy surface [29,30,36,46].

In our in-depth analysis of this problem, we considered for the first time all components contributing to free energy of activation. We have shown that the very large uncertainties in free energies of individual states, which are in the case of type B isomerization as large as 40 kJ/mol, do not cancel significantly even when the corresponding stationary points are carefully chosen so as to be linked by a common intrinsic reaction coordinate. The uncertainty in computed free energy of activation can increase further if the minima and TS configurations are obtained in independent relaxations, as it is often the case in literature. For instance, the computed free energy barrier for the forward mode of type B isomerization spreads over the interval between 36.4 kJ/mol to 97.3 kJ/mol. Counterintuitively, therefore, a gas phase model is indeed likely to provide more reliable results than a periodic model involving zeolite when the static approach is applied to a monomolecular reaction.

The qualitatively correct static gas phase model of type A and B isomerization reactions can be utilized in the interpretation of our MD results. Already from electronic activation energies in gas phase static calculations ($\Delta A_{el}$ in table S3 and S4, 70.4 and 13.7 kJ.mol$^{-1}$ for type B and A isomerization reactions, respectively), the slower rate of type B isomerization with respect to type A isomerization can be deduced. The lower stability of $TS_B$ can be intuitively understood because a larger number of chemical bonds is formed or broken in type

B ($C^2$-$C^4$, $C^3$-$C^4$, $H^a$-$C^3$, and $H^a$-$C^4$) than in type A ($C^3$-$C^2$, $C^3$-$C^4$) isomerization and all those bonds are significantly stretched in $TS_B$ structures compared to the corresponding bond lengths in reactant or product states, see Figure 1.

In the case of type B isomerization, the thermal dependence of free energy of activation is almost exclusively due to the difference in intramolecular contribution to vibrational entropy between reactant and transition state, which is an edge protonated cyclopropane. Such a result is again a consequence of the fact that the atomic motions in transition state are more constrained than those in reactant because a large number of strong chemical bonds are formed or broken in $TS_B$. In the case of type A isomerization, the entropy of activation nearly vanishes which results in a very small variation of the free energy of activation with temperature. In contrast to type B isomerization, the transition state for type A isomerization (a corner protonated cyclopropane) is not significantly more constrained than the reactant because the shifted $CH_3$ group is bound to the rest of molecule (similar to neutral 2,3-dimethyl but-2-ene) by only very loose bonds, which is evident also from the analysis of the MD data (see Sections 3.3.4 and 3.4.4).

In the end, the edge position of the $H^a$ in $TS_B$ (edge-protonated PCP) has both energetic and entropic consequences, causing its lower stability (despite independent stronger bonds, as probed by the vibrational analysis) compared to less constrained $TS_A$. This is the atomic origin of the much higher rate constants found in single-event kinetic models fitted for type A isomerization with respect to type B isomerization [8,15,16].

## 4. CONCLUSION

In this work, a comprehensive ab initio investigation of isomerization reactions of 2,4-dimethyl-pent-2-enium and 2,3,3-trimethyl-but-2-enium cations in chabazite is reported, which provides atomic scale interpretation of the kinetic differences between type A and type

B isomerization of alkenes. The main impacts of our results in terms of understanding of isomerization in heterogeneous catalysis are:

- The proper quantification of the respective free energy barriers of type A and type B isomerization reactions of alkenes by ab initio molecular dynamics, provided here for the first time. The reactions studied herein are the "building blocks" in practice for the key elementary steps of the hydroisomerization of alkanes.
- The unraveling of the origins of the differences in terms of rate constants between type A and B isomerization reactions, in terms of structure of the transition state. A priori, both kinds of TS are protonated cyclopropanes, which makes the ranking in terms of stability difficult without a fine investigation. Our investigation shows that the two TS are very different in nature (tight for type B, an edge-protonated PCP, loose for type A, a corner-protonated PCP), with direct impact on their free energy.

In practice, accurate free energy calculations have been performed by means of molecular dynamics in combination with blue moon ensemble approach [67,68]. The problem with non-ergodic sampling of reactant state due to slow transformation between individual rotational isomers, often overlooked in literature, has been addressed. In the case of type B isomerization, this problem is particularly serious since only one of three symmetrically non-equivalent rotamers can directly undergo the atomic rearrangement associated with this chemical reaction. In this work we proposed and applied a simple solution consisting in explicit sampling of the slow skeletal rotation by the blue moon ensemble approach (other techniques designed to study rare events, such as metadynamics or umbrella sampling, could be used as well [43,80]). The resulting free energy profile is then used to determine the likelihood of the active rotamer among all reactant configurations, which, in combination with the probability density of an arbitrarily chosen reference state of the active rotamer,

779 allows for the determination of the corresponding contribution to free energy changes defined
780 with respect to a generic reactant state.

781 The free energies of activation and reaction computed using MD for type B isomerization
782 at T=300 K are 74.4 kJ/mol and 1.9 kJ/mol, respectively. Increasing temperature to 500 K,
783 which is closer to the conditions relevant for hydrocarbon transformations in zeolite [8,16],
784 the free energy barrier increases to 83.4 kJ/mol, while the free energy of reaction changes
785 only negligibly (3.7 kJ/mol). For type A isomerization, the free energy of activation
786 determined for T=300 K is significantly lower than that for type B isomerization and its
787 numerical value changes only negligibly with T (15.1 kJ/mol (300 K) and 14.0 kJ/mol (500
788 K)). The corresponding kinetic constants determined via the Eyring equation [81] are
789 reported in Scheme 1. Such rate constants, which are compatible in order of magnitude with
790 the rate constants of similar compounds in superacid media[17], are likely to be
791 representative of C7 type A and B isomerization of alkenes between two tertiary carbenium
792 ions.

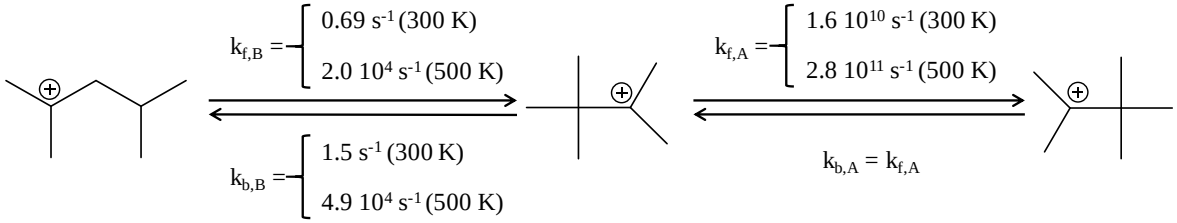


793

794 **Scheme 1.** Kinetic constants at 300 K and 500 K for type B and A isomerization reactions.

795 The former result is consistent with the experimental observation that the measured
796 reaction rate for type A isomerization is several orders of magnitude higher than that for type
797 B isomerization [8,15,16]. As type A isomerization considered in this work leads to
798 formation of product that is symmetry equivalent to reactant, the free energy of reaction is, by
799 definition, zero at all temperatures.

A static calculation analysis appeared to be irrelevant when performed in the zeolite, due to the many stable configurations of different energies that can be found, but insightful when performed for gas phase reactions. Confinement effects indeed appeared to be comparable for the reactants, the transition states and products in our case. The origin of the difference in rate for type A versus type B isomerization reactions was identified on the basis of our calculations: the transition state $TS_A$ (a corner protonated PCP) has a loose structure, with two large C-C bounds at the PCP, and free rotation of the moving methyl group, whereas $TS_B$ (an edge-protonated PCP) is much tighter due to the bridging hydrogen atom, and to the many bonds that are formed or broken at this elementary step.

The simulation protocol developed within this work represents a powerful tool for the investigation of isomerization reactions of alkenes in acidic zeolites and it is currently used to elucidate the more complex mechanisms involving short-lived secondary carbenium ions obtained from proton transfer from zeolite to alkenes. Moreover, the comparison of the transformations of linear to mono-branched, then to di-branched carbenium ions, in comparison with the present di-branched to tri-branched conversion, would be useful to get a more complete view of the full isomerization reaction network. Notably, going beyond DFT may be needed to reach chemical accuracy when describing non-classical species such as the PCP transition states. This was shown for several reactions involving carbenium and carbonium, up to the coupled-cluster level [82–85]. Transposing these approaches to alkene isomerization is a clear perspective to the present work. However, combining this level of calculation with the MD approach is currently prohibitive, so that the problem of the identification by static calculations of ensemble of configurations in the zeolite and ensemble of rotamers for each state in the zeolite needs to be addressed.

**ACKNOWLEDGMENT**

This work was performed using HPC resources from GENCI-IDRIS (Grant 2016-x20160816), the IFPEN ENER110 supercomputer, and the supercomputing infrastructure of Computing Center of the Slovak Academy of Sciences acquired in projects ITMS 26230120002 and 26210120002 supported by the Research and Development Operational Program funded by the ERDF. J.R. thanks Pablo G. Rey for help in writing post-processing scripts. TB acknowledges support from the Slovak Research and Development Agency under the Contract No. APVV−15−0105 and the financial support from IFP Energies nouvelles.

## References

[1] T. Li, K.D. Janda, R.A. Lerner, Nature 379 (1996) 326–327.
[2] W.O. Haag, R.M. Lago, P.B. Weisz, Nature 309 (1984) 589–591.
[3] G.A. Olah, Science 168 (1970) 1298–1311.
[4] J.-I. Yoshida, A. Shimizu, R. Hayashi, Chem. Rev. 118 (2018) 4702–4730.
[5] G.A. Olah, Angew. Chem. Int. Ed. Engl. 34 (1995) 1393–1405.
[6] G.A. Olah, J. Am. Chem. Soc. 94 (1972) 808–820.
[7] J. Zečević, G. Vanbutsele, K.P. de Jong, J.A. Martens, Nature 528 (2015) 245–248.
[8] C. Marcilly, Acido-Basic Catalysis: Application to Refining and Petrochemistry, Technip, 2005.
[9] E. Gutierrez-Acebo, C. Leroux, C. Chizallet, Y. Schuurman, C. Bouchy, ACS Catal. 8 (2018) 6035–6046.
[10] J.A. Martens, D. Verboekend, K. Thomas, G. Vanbutsele, J.-P. Gilson, J. Pérez-Ramírez, ChemSusChem 6 (2013) 421–425.
[11] P.A. Jacobs, M. Dusselier, B.F. Sels, Angew. Chem. Int. Ed. 53 (2014) 8621–8626.
[12] D.-P. Phan, E. Lee, Catalysts 8 (2018) 131.
[13] C. Marcilly, J. Catal. 216 (2003) 47–62.
[14] W. Vermeiren, J.-P. Gilson, Top. Catal. 52 (2009) 1131–1161.
[15] C. Bouchy, G. Hastoy, E. Guillon, J.A. Martens, Oil Gas Sci. Technol. – Rev. IFP Energies nouvelles 64 (2009) 91–112.
[16] J. Weitkamp, ChemCatChem 4 (2012) 292–306.
[17] D.M. Brouwer, Hogeven H., Prog. Phys. Org. Chem. 9 (1972) 179–240.
[18] J. Weitkamp, Ind. Eng. Chem. Prod. Res. Dev. 21 (1982) 550–558.
[19] D.M. Brouwer, J.M. Oelderik, Recl. Trav. Chim. Pays-Bas 87 (1968) 721–736.
[20] P. Raybaud, A. Patrigeon, H. Toulhoat, J. Catal. 197 (2001) 98–112.
[21] E. Gutierrez-Acebo, J. Rey, C. Bouchy, Y. Schuurman, C. Chizallet, ACS Catal. 9 (2019) 1692–1704.
[22] J.D. Petke, J.L. Whitten, J. Am. Chem. Soc. 90 (1968) 3338–3343.
[23] C. Wattanakit, S. Nokbin, B. Boekfa, P. Pantu, J. Limtrakul, J. Phys. Chem. C 116 (2012) 5654–5663.
[24] M.V. Frash, V.B. Kazansky, A.M. Rigby, R.A. van Santen, J. Phys. Chem. B 101 (1997) 5346–5351.
[25] T. Demuth, X. Rozanska, Benco, L.: Hafner, J., R.A. van Santen, H. Toulhoat, J. Catal. 214 (2003) 68–77.

[26] B. Huang, P. Bai, M. Neurock, R.J. Davis, Applied Catalysis A: General 546 (2017) 149–158.
[27] M.A. Natal-Santiago, R. Alcalá, J.A. Dumesic, Journal of Catalysis 181 (1999) 124–144.
[28] V.B. Kazansky, I.N. Senchenya, Journal of Catalysis 119 (1989) 108–120.
[29] J. Hajek, J. van der Mynsbrugge, K. de Wispelaere, P. Cnudde, L. Vanduyfhuys, M. Waroquier, V. van Speybroeck, J. Catal. 340 (2016) 227–235.
[30] P. Cnudde, K. de Wispelaere, J. van der Mynsbrugge, M. Waroquier, V. van Speybroeck, J. Catal. 345 (2017) 53–69.
[31] J.W. Thybaut, L.C.S. Narasimhan, G.B. Marin, J.F.M. Denayer, G.V. Baron, P.A. Jacobs, J.A. Martens, Catal. Lett. 94 (2004) 81–88.
[32] G.G. Martens, G.B. Marin, J.A. Martens, P.A. Jacobs, G.V. Baron, J. Catal. 195 (2000) 253–267.
[33] L.P. de Oliveira, D. Hudebine, D. Guillaume, J.J. Verstraete, J.F. Joly, Oil Gas Sci. Technol. – Rev. IFP Energies nouvelles 71 (2016) 45.
[34] B.D. Vandegehuchte, J.W. Thybaut, G.B. Marin, Ind. Eng. Chem. Res. 53 (2014) 15333–15347.
[35] B.D. Vandegehuchte, J.W. Thybaut, A. Martínez, M.A. Arribas, G.B. Marin, Appl. Catal. A-Gen. 441-442 (2012) 10–20.
[36] T. Bučko, L. Benco, J. Hafner, J.G. Ángyán, J. Catal. 279 (2011) 220–228.
[37] V. van Speybroeck, K. de Wispelaere, J. van der Mynsbrugge, M. Vandichel, K. Hemelsoet, M. Waroquier, Chem. Soc. Rev. 43 (2014) 7326–7357.
[38] P. Cnudde, K. de Wispelaere, L. Vanduyfhuys, R. Demuynck, J. van der Mynsbrugge, M. Waroquier, V. van Speybroeck, ACS Catal. 8 (2018) 9579–9595.
[39] T. Bučko, L. Benco, J. Hafner, J.G. Ángyán, J. Catal. 250 (2007) 171–183.
[40] T. Bučko, L. Benco, O. Dubay, C. Dellago, J. Hafner, J. Chem. Phys. 131 (2009) 214508.
[41] T. Bučko, J. Hafner, J. Phys-Condens. Matter 22 (2010) 384201.
[42] T. Bučko, J. Hafner, J. Catal. 329 (2015) 32–48.
[43] T. Bučko, S. Chibani, J.-F. Paul, L. Cantrel, M. Badawi, Phys. Chem. Chem. Phys. 19 (2017) 27530–27543.
[44] S.L.C. Moors, K. de Wispelaere, J. van der Mynsbrugge, M. Waroquier, V. van Speybroeck, ACS Catal. 3 (2013) 2556–2567.
[45] J. van der Mynsbrugge, A. Janda, S. Mallikarjun Sharada, L.-C. Lin, V. van Speybroeck, M. Head-Gordon, A.T. Bell, ACS Catal. 7 (2017) 2685–2697.
[46] V. van Speybroeck, K. Hemelsoet, L. Joos, M. Waroquier, R.G. Bell, C.R.A. Catlow, Chem. Soc. Rev. 44 (2015) 7044–7111.
[47] A. Janda, B. Vlaisavljevich, L.-C. Lin, S. Mallikarjun Sharada, B. Smit, M. Head-Gordon, A.T. Bell, J. Phys. Chem. C 119 (2015) 10427–10438.
[48] A. Janda, B. Vlaisavljevich, B. Smit, L.-C. Lin, A.T. Bell, J. Phys. Chem. C 121 (2017) 1618–1638.
[49] G. Kresse, J. Hafner, Phys. Rev. B 47 (1993) 558–561.
[50] G. Kresse, J. Hafner, Phys. Rev. B 49 (1994) 14251–14269.
[51] P.E. Blöchl, Phys. Rev. B 50 (1994) 17953–17979.
[52] G. Kresse, D. Joubert, Phys. Rev. B 59 (1999) 1758–1775.
[53] J.P. Perdew, K. Burke, M. Ernzerhof, Phys. Rev. Lett. 77 (1996) 3865–3868.
[54] S. Grimme, J. Comput. Chem. 27 (2006) 1787–1799.
[55] T. Bučko, J. Hafner, S. Lebègue, J.G. Ángyán, J. Phys. Chem. A 114 (2010) 11814–11824.
[56] F. Göltl, A. Grüneis, T. Bučko, J. Hafner, J. Chem. Phys. 137 (2012) 114111.
[57] G. Henkelman, H. Jónsson, J. Chem. Phys. 111 (1999) 7010.

[58] A. Heyden, A.T. Bell, F.J. Keil, J. Chem. Phys. 123 (2005) 224101.
[59] K. Fukui, J. Phys. Chem. 74 (1970) 4161–4163.
[60] K. Fukui, Accounts Chem. Res. 14 (1981) 363–368.
[61] H.P. Hratchian, H.B. Schlegel, J. Phys. Chem. A 106 (2002) 165–169.
[62] W.H. Press, S.A. Teukolsky, W.T. Vetterling, B.P. Flannery, Numerical Recipes in FORTRAN (2Nd Ed.): The Art of Scientific Computing, Cambridge University Press, New York, NY, USA, 1992.
[63] T. Bučko, J. Hafner, J.G. Angyán, J. Chem. Phys. 122 (2005) 124508.
[64] T. Bučko, Theor Chem Acc 137 (2018) 52.
[65] D. Frenkel, B. Smit, Understanding Molecular Simulation: From Algorithms to Applications, Academic Press, 2002, pp. 436-450.
[66] N.E. Henriksen, F.Y. Hansen, Theories of Molecular Reaction Dynamics: The Microscopic Foundation of Chemical Kinetics, Oxford University Press, 2008, pp. 241-261.
[67] E.A. Carter, G. Ciccotti, J.T. Hynes, R. Kapral, Chem. Phys. Lett. 156 (1989) 472–477.
[68] G. Ciccotti, M. Sprik, J. Chem. Phys. 109 (1998) 7737–7744.
[69] T. Bučko, J. Phys-Condens. Matter 20 (2008) 64211.
[70] C. Chipot, A. Pohorille (Eds.), Free Energy Calculations: Theory and Applications in Chemistry and Biology, Springer Berlin Heidelberg, 2007, pp 119-170.
[71] C. Baerlocher, J.K. McCusker, International Zeolite Association, http://www.iza-structure.org/databases/, 2017.
[72] D. Branduardi, F.L. Gervasio, M. Parrinello, J. Chem. Phys. 126 (2007) 54103.
[73] G. Bussi, D. Branduardi, Free-Energy Calculations with Metadynamics: Theory and Practice, Wiley, Hoboken, 2015, pp 1-49.
[74] R. Baron, W.F. van Gunsteren, P.H. Hünenberger, Trends Phys. Chem. 11 (2006) 87–122.
[75] M. Iannuzzi, A. Laio, M. Parrinello, Phys. Rev. Lett. 90 (2003) 238302.
[76] H. Toulhoat, P. Raybaud, E. Benazzi, J. Catal. 221 (2004) 500–509.
[77] A.D. Boese, J.M.L. Martin, J. Chem. Phys. 121 (2004) 3405–3416.
[78] S. Parthiban, J.M.L. Martin, J. Chem. Phys. 114 (2001) 6014–6029.
[79] F. Jensen, Introduction to computational chemistry: Second Edition, 2nd ed., John Wiley & Sons, Chichester England, Hoboken NJ, 2007.
[80] L. Grajciar, C.J. Heard, A.A. Bondarenko, M.V. Polynski, J. Meeprasert, E.A. Pidko, P. Nachtigall, Chem. Soc. Rev. 47 (2018) 8307-8348.
[81] W.F.K. Wynne-Jones, H. Eyring, J. Chem. Phys. 3 (1935) 492–502.
[82] G. Piccini, M. Alessio, J. Sauer, Angew. Chem. Int. Ed. 55 (2016) 5235–5237.
[83] M. Rybicki, J. Sauer, J. Am. Chem. Soc. 140 (2018) 18151–18161.
[84] C. Tuma, J. Sauer, Phys. Chem. Chem. Phys. 8 (2006) 3955–3965.
[85] C. Tuma, T. Kerber, J. Sauer, Angew. Chem. Int. Edit. 49 (2010) 4678–4680.